AgriEngineering

Article

Visualization of Lidar-Based 3D Droplet Distribution Detection for Air-Assisted Spraying

Zhichong Wang [1,2], Yang Zhang [1], Tian Li [2,3,4], Joachim Müller [1] and Xiongkui He [2,3,4,*]

[1] Tropics and Subtropics Group, Institute of Agricultural Engineering, University of Hohenheim, 70599 Stuttgart, Germany; z.wang@uni-hohenheim.de (Z.W.); yang.zhang@uni-hohenheim.de (Y.Z.); joachim.mueller@uni-hohenheim.de (J.M.)
[2] College of Agricultural Unmanned System, China Agricultural University, Beijing 100193, China; cault@cau.edu.cn
[3] College of Science, China Agricultural University, Beijing 100193, China
[4] Centre for Chemicals Application Technology, China Agricultural University, Beijing 100193, China
* Correspondence: xiongkui@cau.edu.cn

Abstract: Air-assisted spraying is a commonly used spraying method for orchard plant protection operations. However, its spraying parameters have complex effects on droplet distribution. The lack of large-scale 3D droplet density distribution measurement methods of equipment has limited the optimization of spraying parameters. Therefore, there is a need to develop a method that can quickly obtain 3D droplet distribution. In this study, a 2D LiDAR was used to quickly scan moving droplets in the air, and a test method that can obtain the visualization of 3D droplet distribution was constructed by using the traveling mode of the machine perpendicular to the scanning plane. The 3D droplet distribution at different positions of the nozzle installed in the air-assisted system was tested at different fan rotation speeds, and the methods for signal processing, point cloud noise reduction, and point cloud division for 2D LiDAR were developed. The results showed that the LiDAR-based method for detecting 3D droplet distribution is feasible, fast, and environmentally friendly.

Keywords: LiDAR; droplet distribution; air-assisted spraying

check for updates

Citation: Wang, Z.; Zhang, Y.; Li, T.; Müller, J.; He, X. Visualization of Lidar-Based 3D Droplet Distribution Detection for Air-Assisted Spraying. *AgriEngineering* **2023**, *5*, 1136–1146. https://doi.org/10.3390/agriengineering5030072

Academic Editors: Marcello Biocca and Roberto Fanigliulo

Received: 30 April 2023
Revised: 13 June 2023
Accepted: 23 June 2023
Published: 3 July 2023

Copyright: © 2023 by the authors. Licensee MDPI, Basel, Switzerland. This article is an open access article distributed under the terms and conditions of the Creative Commons Attribution (CC BY) license (https://creativecommons.org/licenses/by/4.0/).

1. Introduction

Air-assisted spray technology is currently the most widely used pesticide application technology for plant protection in orchards. The basic principle is to deliver pesticide droplets to all parts of the canopy through strong airflow generated by a fan to achieve droplet deposition uniformly and improve pesticide efficacy [1]. The airflow of the fan not only increases the droplet deposition inside the canopy by opening the branches and leaves outside the canopy, but it also raises the adhesion of the pesticide droplets on the back of the leaves as a consequence of promoting the swing of the branches and leaves. In traditional orchard air-assisted sprayers and tower sprayers, adjustments to the wind field are typically made by modifying the length and angle of the deflector, as well as the mounting position. However, multi-channel orchard air-assisted sprayers provide more precise wind field adjustments by enabling the adjustment of the position and spray angle of each outlet. As the research in the field of air-assisted spraying has progressed, an increasing number of parameters have been found to be related to its effect, which has made it challenging to determine the optimal design of air-assisted spraying [2].

The conventional method for testing spray distribution in orchards was carried out based on the amount of droplet deposition, mainly using a vertical deposition distribution test bench [3]. However, this test method requires multiple tests at various distances to obtain a two-dimensional spatial distribution, and obtaining a three-dimensional spatial distribution is challenging. Due to the high cost of actual testing and the difficulty of reproducing the environment, much of the optimization work for the orchard sprayer

was based on computational fluid dynamics (CFD). CFD-based technology can realize the simulation of two-phase flow to achieve the tracking of droplet particles and calculate the results of droplet spatial distribution [4,5], but there is still a discrepancy between CFD simulation outcomes and actual results [6].

Laser imaging is an imaging measurement technique that utilizes the reflection of particles in the air against an emitted light source. The most common laser imaging techniques include particle droplet image analysis (PDIA) and particle image velocimetry (PIV). PDIA uses a laser or monochromatic light source as a background to rapidly capture high-resolution images of droplets which are then identified and analyzed for the size, velocity, and direction of droplet motion using two consecutive teens [7,8]. However, the observable field of view of PDIA is too small to track a large range of droplets, and PDIA can only analyze droplets within the focal plane. On the other hand, PIV is a technique for the velocity analysis of droplet particles within the laser plane using high-speed photography, and this method has higher requirements for the camera as well as for the purity of the background during the computation [9,10].

LiDAR technology has been applied in agriculture as early as 1984 [11]. Since then, with the continuous advancement and optimization of LiDAR technology, its widespread adoption in agriculture has been increasingly observed [12–15]. Particularly in the 21st century, LiDAR technology has developed rapidly, and at the same time, with the gradual popularization of unmanned vehicles, the price of LiDAR has been gradually reduced, which makes it popular in agriculture, an extremely cost-conscious field. The multipurpose function of LiDAR is also gradually being explored, for example, Seol et al. achieved simultaneous target and drift detection using LiDAR mounted on a variable rate sprayer, showcasing its potential to optimize pesticide application and minimize environmental impact [16,17].

For drift testing, the use of lidar for spray drift testing was investigated in 1997, where the LiDAR was mounted on a horizontal and vertical rotating mechanism, respectively. This was achieved by scanning in a 2D plane using a pulsed LiDAR and using the LiDAR reflection signal intensity to obtain a 2D measurement of the plume [18]. However, the research on spray 3D distribution is currently focused more on drift measurement [19,20], with less emphasis on spray droplets. Li et al. used 3D LiDAR to achieve the droplet distribution measurement of a single nozzle and performed quantitative analysis [21], and Boqin Liu et al. used 3D LiDAR to perform droplet detection on the air-assisted unit and fitted the deposition based on the droplet density distribution [22]. However, there is still a lack of research on the processing of LiDAR visualization effects.

Therefore, this study proposed a visualization method based on LiDAR for droplet distribution measurement technology. By moving the machine perpendicular to the LiDAR scanning plane, the 2D LiDAR scanning data were reconstructed into a 3D spatial distribution. The three different installed nozzle positions and three different fan speeds were adjusted, the noise and background of the point cloud were removed, and the point cloud was aligned. The reconstructed 3D spatial distribution of the droplet cloud provides a fast, inexpensive, and visualized method for structural and application parameter settings for orchard air-assisted sprayers and similar machines.

2. Material and Method

2.1. Installation of LiDAR

The LiDAR (LMS111, Sick, Waldkirch, Germany) was mounted on a tripod at a height of 2.35 m above the ground, and the maximum detection of the LiDAR range is 20 m. The communication cable and power cable (12 V DC) were then connected to the device. The LiDAR was fixed on the tripod after rotating 90 degrees, and the vertical direction of the LiDAR was set as the X-axis parallel to the ground, and the vertical direction from the ground was set as the Z-axis. The travel route of the machine was planned 6 m away from the LiDAR, and the travel route was not less than 6 m. The travel direction is set as the Y-axis, perpendicular to the detection plane (XOZ), so as to establish a three-dimensional

coordinate system. The LiDAR scanning frequency was set to 25 Hz, and the scanning angle was set at −45~225° with a 0.25° interval. The first echo signal was selected, and the fog filter was turned off.

2.2. Spraying System

The spraying system utilized in this experiment consisted of 3 main components: the air-assisted system, the liquid pump, and the nozzle. The air-assisted system includes a brushless motor (X5212S, Sunnysky, Columbus, OH, USA), a carbon fiber propeller (2055, T-Motor, Nanchang, China), an electronic speed controller (X-Rotor 80A-HV, Hobbywing, Shenzhen, China), and a motor signal generator (DC6. HJ Facalhobby, Shenzhen, China). The nozzle used was a TR8004 (Lechler, Metzingen, Germany) operating at a pressure of 0.3'MPa. To achieve 3D space detection with a 2D LiDAR, it is necessary to move the machine or LiDAR in a direction perpendicular to the scanning plane to obtain a similar result to CT tomography, which can then be reconstructed in 3D space. The whole system was powered by 220 V and the operator pushed the system along the predetermined route at a forward speed of 0.5 m/s, which is the Y direction in Figure 1. In this test, the fan was set at 1500 rpm, 2500 rpm, and 3500 rpm, and the axial wind speeds at 50 cm were 3 m/s, 7 m/s, and 10 m/s. The nozzle positions were provided with three mounting heights located at the edge of the fan: above the axis (H1), at the center of the axis (H2), and below the axis (H3), as shown in Figure 2. All spraying tests were conducted at night with an ambient wind speed of less than 0.5 m/s.

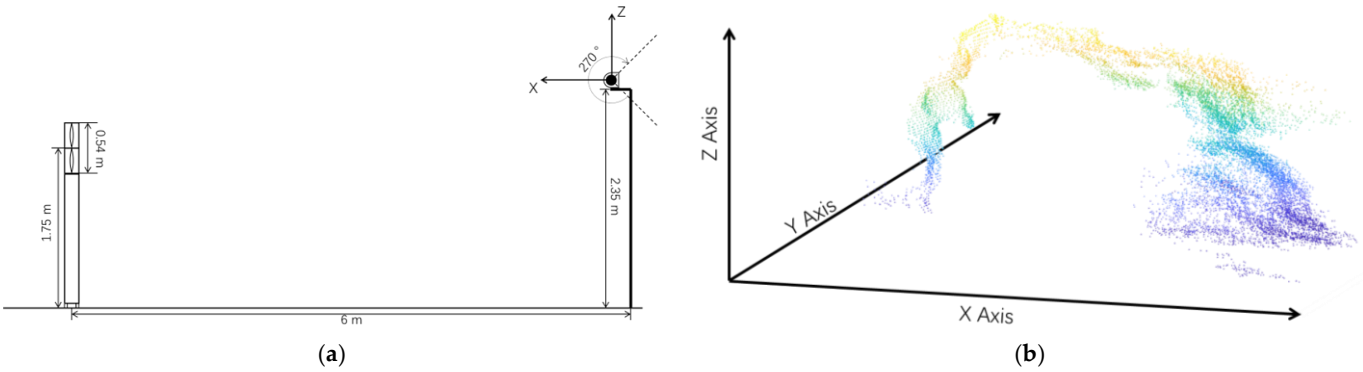

Figure 1. (**a**) LiDAR and sprayer setup layout (XOZ plane). Dotted line is the detected range of LiDAR (from 45~315° in XOZ plane). (**b**) Sprayer and droplet cloud in XYZ coordinate system. Color means the heights from yellow (highest) to blue (lowest).

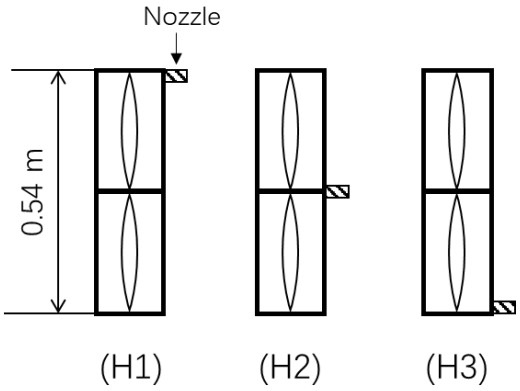

Figure 2. Nozzle setup layout. Above the axis (H1), center of the axis (H2), below the axis (H3).

2.3. Data Processing

2.3.1. Point Cloud Calculation from LiDAR

All data processing was performed in MATLAB 2022b (MathWorks, Natick, MA, USA) (CPU i7-8559U, RAM 32 GB). The XYZ coordinates of the point cloud were calculated based on the time and distance information obtained from the LiDAR data, as shown in Equations (1)–(3):

$$X_i = D_i \cdot \sin(\alpha_i) \quad (1)$$

$$Y_i = T_i \cdot v \quad (2)$$

$$Z_i = D_i \cdot \cos(\alpha_i) \quad (3)$$

where D_i and T_i are the original LiDAR data, which are the distance from point i to LIDAR, "mm"; scanning time, "ms". α_i is the scanning angle, which is known by checking the table in the manual, "°". v is the traveling speed of the machine, which is 0.5 m/s in this experiment.

Figure 3a,e shows the original point cloud data. The test region of interest (ROI) was selected, and the range was set to $-2000 < X < 8000$ mm. The preliminary ground fit was performed using the pcfitplane function [23]; the reference vector was set to [0, 0, 1], the and ROI range was set to $\min(Z) < Z < \min(Z) + 200$, and the ground splitting result is shown in Figure 3b,f. The ground obtained from the splitting process was compressed in the XOZ plane, and the ground slope was obtained by linear fitting and the ground tilt angle β. The point cloud was then rotated by β degrees around the y-axis using a transformation matrix [23]. The ground was re-fitted to the rotated point cloud using the pcfitplane function [24] with the same parameters as the first fit. The result of this second fit was shown in Figure 3c,g. The split ground information was then deleted and only the non-ground information was retained. The non-ground information was rotated by -β degrees around the y-axis using the transformation matrix to recover the droplet point cloud information, as shown in Figure 3d,h.

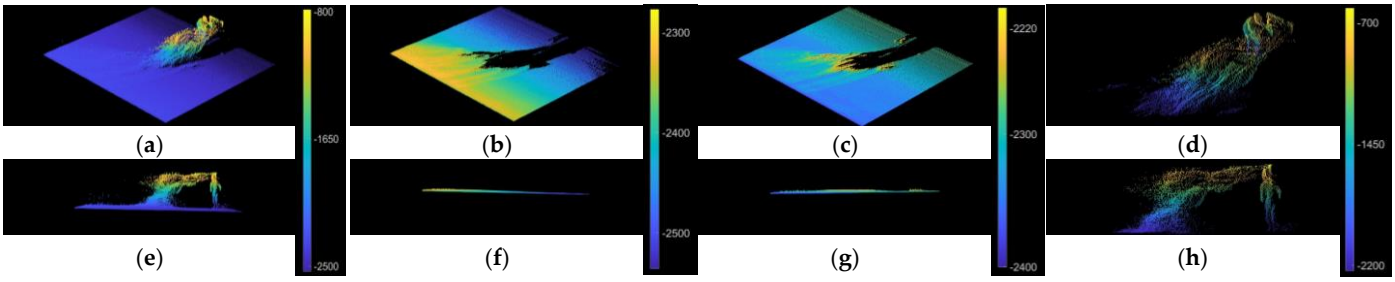

Figure 3. Point cloud results during the data processing, where (**a**–**d**) viewed at 45° from moving direction; (**e**–**h**) viewed at front direction (Y-axis). And (**a**,**e**) were original point cloud, (**b**,**f**) were after first ground fit, (**c**,**g**) were after second ground fit and rotating, and (**d**,**h**) were the non-ground results. Color means height (mm) from yellow (highest) to blue (lowest). Black is the background color to enhance the show, which has no meaning.

The pcsegdist function was used to remove the discrete noise points [25], with a minimum distance threshold of 500 mm. The part above $X > 6000$ mm is divided as the machine part, and the coordinate points [X_s, Y_s, Z_s] of the machine head are derived. The [X_s, Y_s, 0] point is set as the origin of the coordinate system by Equations (4)–(6).

$$X_i' = X_i - X_s \quad (4)$$

$$Y_i' = Y_i - Y_s \quad (5)$$

$$Z_i' = Z_i + Z_g \quad (6)$$

where the constant Z_g in the z-axis calculation is the height from the ground, which is 2350 mm in this experiment.

2.3.2. Triangulation for Point Cloud of Droplet

All point clouds were gridded at 100 mm intervals, and the duplicate data were removed. The detailed running code is shown in Code S1. The internal point cloud of the spray body was removed to retain only the surface points (Point Cloud S1). The surface points were triangulated using the alphaTriangulation function [26], and the triangulated results were subjected to Laplace smoothing [27].

3. Results

3.1. Segmentation Points Cloud

The point cloud splitting results are shown in Figure 4, with the ground rendered in white, the machine and operator in red, and the spray droplet portion represented by a gradient from yellow to blue, indicating different heights, with yellow being the highest and blue the lowest. The 3D display is shown in Video S1. It can be seen that the ground separation results were good, except for the R3200-H3 treatment, where some of the ground was not correctly identified. But almost all of the ground was identified accurately in the other treatments. For the machine and the operator, the results of the three iterations of the overlay are in the same position and the machine is correctly identified. The shape of the spray droplets was also more direct and clearer, which can effectively describe the spray droplet distribution for the different parameters.

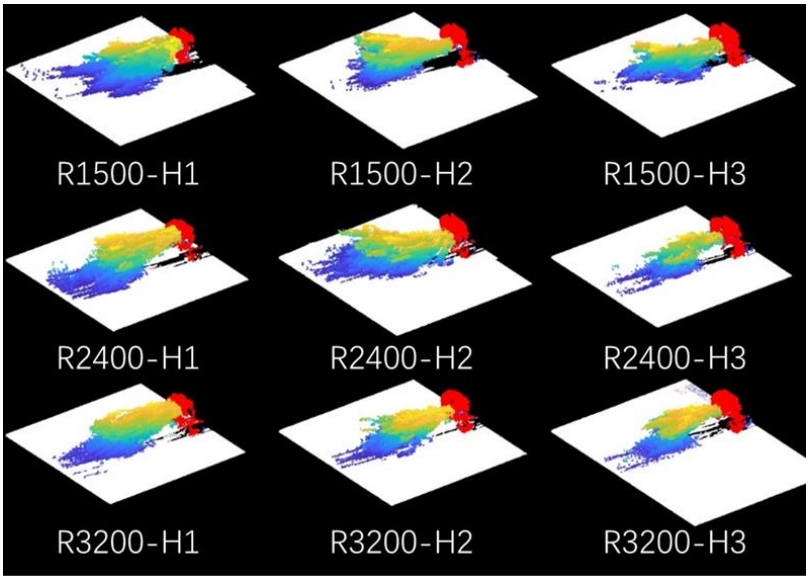

Figure 4. Integration result of 3 times repetition for all parameters, where white points mean the points from ground, red points mean the points from sprayer and operator, and the colorful points mean the points from droplet cloud. Where R1500 means the rotor speed is 1500 rpm; H1, H2, and H3 means different nozzle installed position at the top, middle, and bottom, respectively.

3.2. Repeatability of Multiple Spraying

The high overlap between the sprayer head and the operator in the three replicates provides evidence that using the head of the implement as the origin of the coordinate axis is a valid approach. By using the coordinate system with the sprayer head as the origin of the axis, the droplets from three different replicates exhibited good agreement (Figure 5, Video S2), indicating the reproducibility of this test method. Moreover, the shape of the spray from the same machine was approximately consistent, and the trajectories were similar in both spray distance (X direction) and travel direction (Y direction).

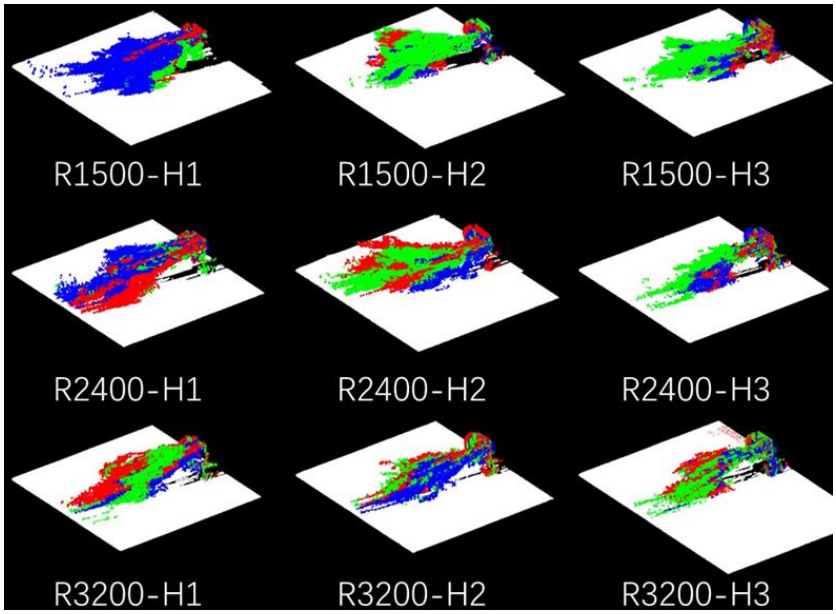

Figure 5. Integration result of 3 times repetition for all parameters, where white points mean the points from ground, red points mean the points from 1st repetition, green points mean the points from 2nd repetition, and the blue points mean the points from 3rd repetition.

3.3. Triangulation of Different Parameters

Figure 6 illuminates the results of the triangulation of different nozzle installation positions at varying fan speeds. The transparency setting of the droplet cloud indicates that the opaquer part is denser, whereas the less dense part is represented by the edge of the droplet cloud. In Figure 6a–c, the initial position of spray marked in a different color could tell the nozzle position correctly. The red color shows that the nozzle was installed in the upper part of the wind-fed spray and its droplet cloud starts higher than the green (H2, center) and blue (H3, bottom). And the rotation speed at a low speed (R1500) and high speed (R3200) did not significantly affect the wind-fed distance in the range of 1.8–4.5 m in the wind direction. However, in the top view of direction, the mounting height had little effect on the droplet cloud pattern under low-speed conditions (Figure 6d). Under medium- and high-speed conditions (Figure 6e,f), the higher the mounting height, the more backward the droplet cloud moved relative to the direction of travel. This result indicates that the transport of droplets was faster at higher mounting heights.

The effect of the fan speed at the different nozzle installation was shown in Figure 7. When the nozzle is installed on top (H1), increasing the fan speed from 1500 rpm to 2400 rpm can significantly increase the wind speed distance (Figure 7a) and reduce the backward distance of the droplets (Figure 7d), which can help the droplets reach the target faster and reduce potential drift. However, increasing the fan speed to 3200 rpm will not improve the range any further. When the nozzle is installed in the center (H2), the effect of changing the fan speed on droplet transport is not very significant (Figure 7b,e)). When the nozzle is installed at the bottom (H3), increasing the fan speed can slightly reduce the backward movement (Figure 7f).

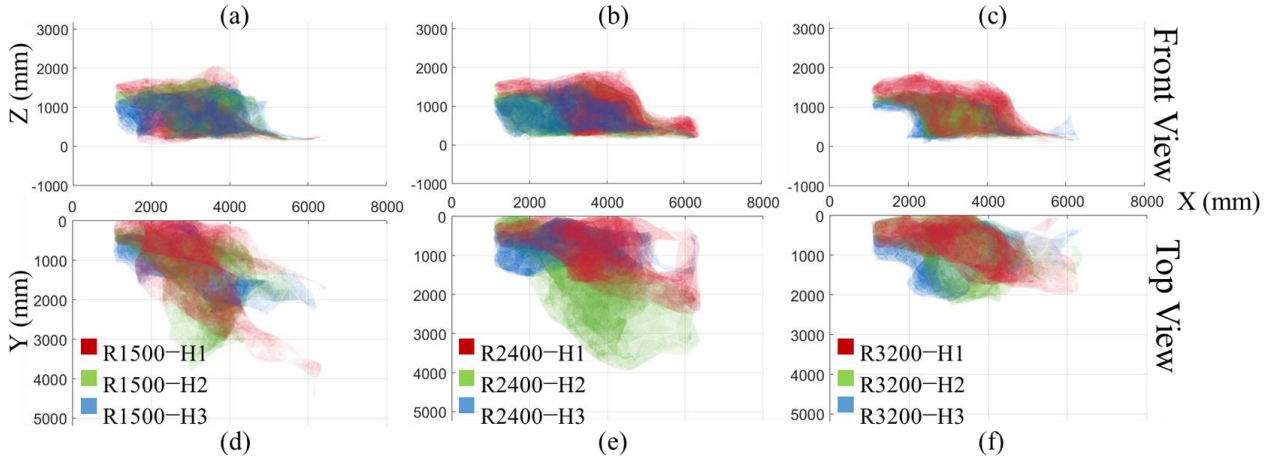

Figure 6. Front view (**a**–**c**) and top view (**d**–**f**) of three different nozzle position under different rotor speed, where R1500 means the rotor speed is 1500 rpm; H1, H2, and H3 means different nozzle installed position at the top, middle, and bottom, respectively.

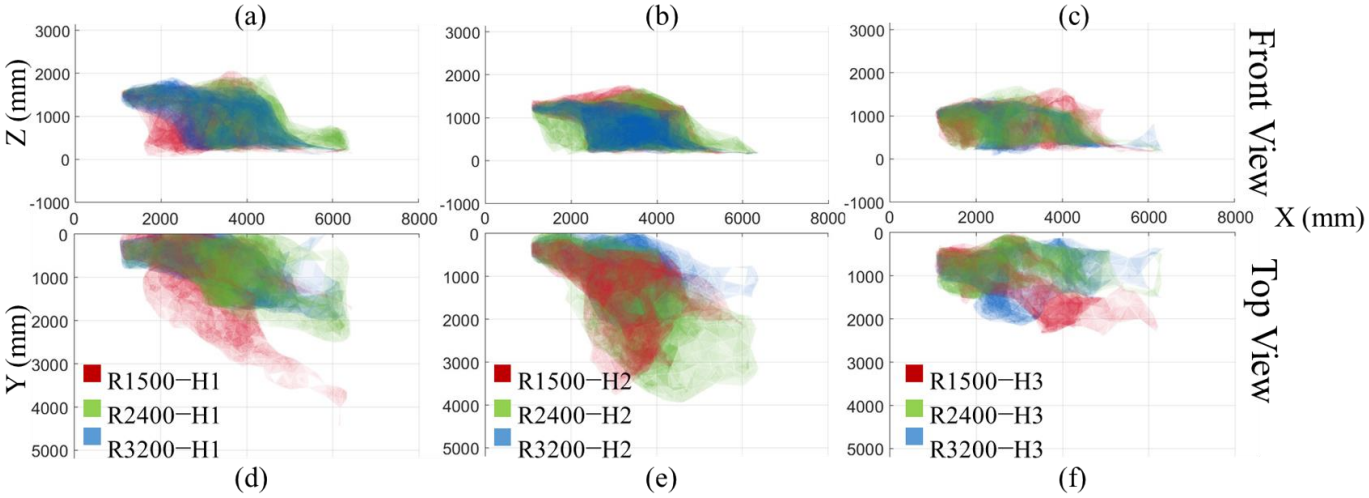

Figure 7. Front view (**a**–**c**) and top view (**d**–**f**) of three different rotor speed under different nozzle position, where R1500 means the rotor speed is 1500 rpm; H1, H2, and H3 means different nozzle installed position at the top, middle, and bottom, respectively.

4. Discussion

4.1. Droplet Distribution

Due to the lack of large-scale three-dimensional droplet distribution test methods, the development and parameter adjustment of orchard air-driven sprayers can only be carried out through droplet deposition tests. However, the test in the actual orchard needs to consume a lot of manpower and material costs. At the same time, due to the influence of the canopy growth cycle, a large number of test samples are required to improve the test accuracy. Therefore, a new method of droplet distribution visualization based on LiDAR-based droplet detection was proposed. Although quantitative analysis was not performed in this study, certain patterns could still be found by the variation in different parameters.

Normally, the nozzle was installed in the center of the air-assisted unit, but this is not always correct, i.e., the nozzle installed at the top (H1) can help the droplet delivery at the 2400 rpm fan speed (R2400), as shown in Figure 6b, as well as reduce the backward direction drift, as shown in Figure 6e. Three different fan speeds were set, but the delivery distance did not always increase with the higher fan speed (Figure 7), which is an important and valuable point that can save a lot of energy. This phenomenon can give manufacturers and users some ideas to improve the air-assisted sprayer.

This detection method is also applicable to the air delivery system of the axial fan, as well as the latest multi-unit air delivery spray system. It will greatly shorten the time for tool design parameters and spray parameter optimization. Compared with the traditional field test, this method is faster and does not require consumables. Also, the calculation method does not require a large computing power compared with CFD technology. In addition, with the recent popularization of unmanned vehicle technology, the price of LiDAR has gradually decreased. This research has good generalization and universality.

Current studies using LiDAR to detect droplets tend to focus on drift rather than droplets. The main methods used to quantify the distribution are droplet density [17,20,22,28] and emission intensity [29,30]. Since the spatial density of droplets cloud is much higher than that of drift, it is not easy for droplets to obscure droplets in the drift test, and the depth of the test field is sufficient to achieve droplet density detection over a larger area. However, for the detection of droplet distribution, the simultaneous detection of multiple locations may be required, and the algorithm will be fused to finally meet the all-around accurate detection of spatial distribution. While some LiDAR sensors can record multiple echo signals, potentially resolving mutual occlusion between droplets, this may also increase noise signals due to transmission and complex reflection within the droplet cloud, thereby exacerbating subsequent visualization processing difficulties.

Meanwhile, the reflection intensity of LiDAR is easily affected by the detection angle [21]. There has been even more in-depth research in the field of meteorology for the LiDAR detection of water droplet clouds [31]. The difference in the size and detection distance between these kind of raindrops and spray droplets is large, which can only provide partial theoretical support and cannot be directly applied to the field of agricultural spraying.

In conclusion, there are still many problems to be studied and worthy of research in the fog droplet distribution detection method of lidar in the future. Based on the visualization method of this study, the feasibility of this method has been preliminarily proven, and a series of application scenarios have been proposed and better prospects have been made.

4.2. LiDAR Droplet Detection Method

Because of the limitations of the current actual test methods, this test cannot be used as a confirmatory test, but the accuracy of this test can still vary from some aspects. For example, the spray start position can be clearly observed in Figures 6 and 7. The droplet cloud with the nozzle installed at the top (H1) started at about 1600 mm from the ground, as shown in Figure 7a; the nozzle installed at the center (H2) started at about 1350 mm, as shown in Figure 7b; and the nozzle installed at the bottom (H3) started at about 1100 mm, as shown in Figure 7c. This is consistent with the designed installation position of the nozzle (Figure 2), and the pattern is also consistent at the three different fan speeds, where the start positions almost completely overlap.

Whilst the size of the LiDAR (LMS111) spot diameter is approximately 1 mm, the size of agricultural spraying droplets is generally between 100 and 500 µm. When the spot is larger than the droplet particles, some of the laser light is reflected back to the LiDAR, while some of the laser light still passes through or bypasses the droplets. Therefore, the fog filter setting needs to be turned off in the LIDAR to prevent interference. For other LiDAR models, the fog droplets can be detected by selecting to accept the first reflection since they are the closest detected object. It is important to note that the LiDAR only records the first reflected light, resulting in a better detection effect for the surface of the droplet cloud closer to the LiDAR side compared to the inner and distal droplets cloud relative to the LiDAR. This effect can be observed in Figure 3b,c, where a shadow on the ground is visible after removing the droplet cloud. This shadow suggests that the LiDAR cannot fully penetrate the droplet cloud to detect objects on the other side, indicating a limitation in its detection capabilities. In light of the LiDAR's limited ability to detect objects beyond the surface of the droplet cloud near its side, there may be decreased detection efficacy for droplet cloud objects further from the LiDAR. As evidenced in Figure 7b, there is minimal

variation in the 0–2 m range with an increasing fan speed, although this may be due to the reduced detectability of the LiDAR at this distance. Thus, careful consideration must be given to interpreting LiDAR data, particularly when evaluating objects located far from the LiDAR's position.

4.3. Accuracy of 3D Model Based on Evaluated Speed

According to Equation (2), the Y-axis data are calculated by speed and time, and the time recording is completed by the LiDAR itself, which has a high accuracy. The accuracy of the Y-axis is mainly affected by the forward speed; therefore, the forward speed used for scanning is crucial for achieving accurate results. The forward speed should be stable, and the operator must practice several times to achieve a stable forward speed. Higher forward speeds result in larger distances between scanning layers and lower spatial resolution. Conversely, lower forward speeds result in longer scanning times and higher static requirements for the scanned object. In addition, unstable environmental conditions may negatively impact the results obtained with lower forward speeds. To ensure accurate scanning of the droplet cloud, it is crucial to maintain its stability and stationary position during the scanning process. Therefore, the scanning should be conducted under stable environmental conditions, as was done in this study by selecting almost windless conditions. However, under windy conditions, it may be necessary to increase the number of repetitions and superimpose the results to obtain the final distribution, or to increase the step speed to reduce the scanning time. In this case, the LiDAR scanning frequency should be increased and the angular resolution reduced to compensate for the decrease in spatial resolution in the direction of the driving axis caused by increasing the step speed, i.e., sacrificing resolution in the scanning plane to improve resolution in the driving direction.

5. Conclusions

In this study, a LiDAR-based method was proposed for visualizing the 3D distribution of droplets in wind-driven spraying. The method involved scanning the droplet distribution at three different fan rotation speeds for three different nozzle installation positions using 2D LiDAR. The point cloud results were divided and noise was reduced for the open environment, and triangulation was performed to visualize the shape of the droplet cloud based on the fusion of multiple scans. The results showed that the proposed method was feasible, had good reproducibility, and the effect of different spray parameters on the droplet distribution could be analyzed based on the triangulation results. Although this study did not perform actual test verification, it still presents and discovers some regularities through experiments. Compared to the other measurement and simulation methods of the droplet distribution, the LiDAR results provided excellent visualization without requiring consumables or indicators, making it an environmentally friendly and fast detection method. However, more research is still needed to evaluate the accuracy of LiDAR for droplet distribution results, especially the experimental quantitative comparison of droplet density.

Supplementary Materials: The following supporting information can be downloaded at: https://www.mdpi.com/article/10.3390/agriengineering5030072/s1, Code S1: Triangulation processing; point cloud S1: Surface points cloud R1500 H1; Video S1: Figure 4; Video S2: Figure 5.

Author Contributions: Z.W.: conceptualization, investigation, methodology, validation, and writing—original draft. Y.Z.: conceptualization, investigation, and writing—review and editing. T.L.: conceptualization and investigation. J.M.: supervision and review. X.H.: supervision and funding acquisition. All authors have read and agreed to the published version of the manuscript.

Funding: This study was financially supported by the earmarked fund for CARS: CARS-28, the 2115 Talent Development Program of China Agricultural University, Sanya Institute of China Agricultural University Guiding Fund Project (Grant No. SYND-2021-06).

Data Availability Statement: To verify the possibility of using the data available in the Supplementary Materials or the images collected, please contact the first author.

Acknowledgments: The authors would like to thank Guoyi Ma for their support in the measurement.

Conflicts of Interest: The authors declare no conflict of interest.

References

1. Liu, L.; Liu, Y.; He, X.; Liu, W. Precision Variable-Rate Spraying Robot by Using Single 3D LIDAR in Orchards. *Agronomy* **2022**, *12*, 2509. [CrossRef]
2. Li, T.; Qi, P.; Wang, Z.; Xu, S.; Huang, Z.; Han, L.; He, X. Evaluation of the Effects of Airflow Distribution Patterns on Deposit Coverage and Spray Penetration in Multi-Unit Air-Assisted Sprayer. *Agronomy* **2022**, *12*, 944. [CrossRef]
3. Wegener, J.K.; von Hörsten, D.; Pelzer, T.; Osteroth, H.J. Basic Research into Different Parameters Influencing the Quality of Vertical Distribution by Crop Sprayers. *Landtechnik* **2016**, *71*, 4–13. [CrossRef]
4. Dekeyser, D.; Duga, A.T.; Verboven, P.; Endalew, A.M.; Hendrickx, N.; Nuyttens, D. Assessment of Orchard Sprayers Using Laboratory Experiments and Computational Fluid Dynamics Modelling. *Biosyst. Eng.* **2013**, *114*, 157–169. [CrossRef]
5. Duga, A.T.; Delele, M.A.; Ruysen, K.; Dekeyser, D.; Nuyttens, D.; Bylemans, D.; Nicolai, B.M.; Verboven, P. Development and Validation of a 3D CFD Model of Drift and Its Application to Air-Assisted Orchard Sprayers. *Biosyst. Eng.* **2017**, *154*, 62–75. [CrossRef]
6. Duga, A.T.; Dekeyser, D.; Ruysen, K.; Bylemans, D.; Nuyttens, D.; Nicolai, B.M.; Verboven, P. Numerical Analysis of the Effects of Wind and Sprayer Type on Spray Distribution in Different Orchard Training Systems. *Bound. Layer Meteorol.* **2015**, *157*, 517–535. [CrossRef]
7. Kashdan, J.T.; Shrimpton, J.S.; Whybrew, A. Two-Phase Flow Characterization by Automated Digital Image Analysis. Part 2: Application of PDIA for Sizing Sprays. *Part. Part. Syst. Charact.* **2004**, *21*, 15–23. [CrossRef]
8. Kashdan, J.T.; Shrimpton, J.S.; Whybrew, A. A Digital Image Analysis Technique for Quantitative Characterisation of High-Speed Sprays. *Opt. Lasers Eng.* **2007**, *45*, 106–115. [CrossRef]
9. De Cock, N.; Massinon, M.; Nuyttens, D.; Dekeyser, D.; Lebeau, F. Measurements of Reference ISO Nozzles by High-Speed Imaging. *Crop Prot.* **2016**, *89*, 105–115. [CrossRef]
10. Dorr, G.J.; Hewitt, A.J.; Adkins, S.W.; Hanan, J.; Zhang, H.; Noller, B. A Comparison of Initial Spray Characteristics Produced by Agricultural Nozzles. *Crop Prot.* **2013**, *53*, 109–117. [CrossRef]
11. Krabill, W.B.; Collins, J.G.; Link, L.E.; Swift, R.N.; Butler, M.L. Airborne Laser Topographic Mapping Results. *Photogramm. Eng. Remote Sens.* **1984**, *50*, 685–694.
12. Chen, Y.; Zhu, H.; Ozkan, H.E. Development of LIDAR-guided sprayer to synchronize spray outputs with canopy structures. In Proceedings of the American Society of Agricultural and Biological Engineers Annual International Meeting, Louisville, KY, USA, 7–10 August 2011; American Society of Agricultural and Biological Engineers: St. Joseph, MI, USA, 2011; Volume 1, pp. 11–24.
13. Gené-Mola, J.; Gregorio, E.; Guevara, J.; Auat, F.; Sanz-Cortiella, R.; Escolà, A.; Llorens, J.; Morros, J.-R.R.; Ruiz-Hidalgo, J.; Vilaplana, V.; et al. Fruit Detection in an Apple Orchard Using a Mobile Terrestrial Laser Scanner. *Biosyst. Eng.* **2019**, *187*, 171–184. [CrossRef]
14. Qiu, Q.; Sun, N.; Bai, H.; Wang, N.; Fan, Z.; Wang, Y.; Meng, Z.; Li, B.; Cong, Y. Field-Based High-Throughput Phenotyping for Maize Plant Using 3d LIDAR Point Cloud Generated with a "Phenomobile". *Front. Plant Sci.* **2019**, *10*, 554. [CrossRef] [PubMed]
15. Han, L.; Wang, S.; Wang, Z.; Jin, L.; He, X. Method of 3D Voxel Prescription Map Construction in Digital Orchard Management Based on LiDAR-RTK Boarded on a UGV. *Drones* **2023**, *7*, 242. [CrossRef]
16. Seol, J.; Kim, J.; Son, H. Il Field Evaluations of a Deep Learning-Based Intelligent Spraying Robot with Flow Control for Pear Orchards. *Precis. Agric.* **2022**, *23*, 712–732. [CrossRef]
17. Seol, J.; Kim, J.; Son, H. Il Spray Drift Segmentation for Intelligent Spraying System Using 3D Point Cloud Deep Learning Framework. *IEEE Access* **2022**, *10*, 77263–77271. [CrossRef]
18. Stoughton, T.E.; Miller, D.R.; Yang, X.; Ducharme, K.M. A Comparison of Spray Drift Predictions to Lidar Data. *Agric. For. Meteorol.* **1997**, *88*, 15–26. [CrossRef]
19. Gregorio, E.; Torrent, X.; Planas, S.; Rosell-Polo, J.R. Assessment of Spray Drift Potential Reduction for Hollow-Cone Nozzles: Part 2. LiDAR Technique. *Sci. Total Environ.* **2019**, *687*, 967–977. [CrossRef]
20. Li, L.; Zhang, R.; Chen, L.; Liu, B.; Zhang, L.; Tang, Q.; Ding, C.; Zhang, Z.; Hewitt, A.J. Spray Drift Evaluation with Point Clouds Data of 3D LiDAR as a Potential Alternative to the Sampling Method. *Front. Plant Sci.* **2022**, *13*, 939733. [CrossRef]
21. Tian, L.; Xiongkui, H.; Zhichong, W.; Huang, Z.; Han, L. Method for Measuring the 3D Spatial Distribution of Spray Volume Based on LIDAR. *Trans. Chin. Soc. Agric. Eng.* **2021**, *37*, 42–49. [CrossRef]
22. Liu, B.; Li, L.; Zhang, R.; Tang, Q.; Ding, C.; Xu, G.; Hewitt, A.J.; Chen, L. Analysis of the Spatial and Temporal Distribution of a Spray Cloud Using Commercial LiDAR. *Biosyst. Eng.* **2022**, *223*, 78–96. [CrossRef]
23. Mathworks Matrix Representation of Geometric Transformations. Available online: https://ww2.mathworks.cn/help/releases/R2022b/images/matrix-representation-of-geometric-transformations (accessed on 27 March 2023).
24. Torr, P.H.S.; Zisserman, A. MLESAC: A New Robust Estimator with Application to Estimating Image Geometry. *Comput. Vis. Image Underst.* **2000**, *78*, 138–156. [CrossRef]
25. Mathworks Pcsegdist. Available online: https://ww2.mathworks.cn/help/releases/R2022b/vision/ref/pcsegdist.htm (accessed on 27 March 2023).

26. Mathworks AlphaTriangulation. Available online: https://ww2.mathworks.cn/help/releases/R2022b/matlab/ref/alphashape.alphatriangulation.html (accessed on 27 March 2023).
27. Zhang, Y.; Hamza, A. Vertex-based anisotropic smoothing of 3D mesh data. In Proceedings of the 2006 Canadian Conference on Electrical and Computer Engineering, Ottawa, ON, Canada, 7–10 May 2006; pp. 202–205.
28. Gil, E.; Llorens, J.; Llop, J.; Fàbregas, X.; Gallart, M. Use of a Terrestrial LIDAR Sensor for Drift Detection in Vineyard Spraying. *Sensors* **2013**, *13*, 516–534. [CrossRef] [PubMed]
29. Gregorio, E.; Rosell-Polo, J.R.; Sanz, R.; Rocadenbosch, F.; Solanelles, F.; Garcerá, C.; Chueca, P.; Arnó, J.; del Moral, I.; Masip, J.; et al. LIDAR as an Alternative to Passive Collectors to Measure Pesticide Spray Drift. *Atmos. Environ.* **2014**, *82*, 83–93. [CrossRef]
30. Gregorio, E.; Rocadenbosch, F.; Sanz, R.; Rosell-Polo, J. Eye-Safe Lidar System for Pesticide Spray Drift Measurement. *Sensors* **2015**, *15*, 3650–3670. [CrossRef]
31. Sassen, K.; Zhao, H. Lidar Multiple Scattering in Water Droplet Clouds: Toward an Improved Treatment. *Opt. Rev.* **1995**, *2*, 394–400. [CrossRef]

Disclaimer/Publisher's Note: The statements, opinions and data contained in all publications are solely those of the individual author(s) and contributor(s) and not of MDPI and/or the editor(s). MDPI and/or the editor(s) disclaim responsibility for any injury to people or property resulting from any ideas, methods, instructions or products referred to in the content.